catalysts

MDPI

Article

Post-Synthesis Ion Beam Sputtering of $Pt/CeO_2–ZrO_2$ Catalysts: Correlating Surface Modifications with Light-Off Performance

Ruairi O'Donnell [1], Marina Maddaloni [2,3], Salvatore Scaglione [4] and Nancy Artioli [2,3,*]

[1] School of Chemistry and Chemical Engineering, Queen's University Belfast, David-Keir Building, Stranmillis Road, Belfast BT9 5AG, UK; rodonnell17@qub.ac.uk
[2] CEEP Laboratory, Department of Civil Engineering, Architecture, Territory, Environment and Mathematics, University of Brescia, Via Branze 38, 25123 Brescia, Italy; marina.maddaloni@unibs.it
[3] Consorzio Interuniversitario Nazionale per la Scienza e Tecnologia dei Materiali (INSTM), University of Brescia, Via Branze 38, 25123 Brescia, Italy
[4] ENEA-CRE Casaccia, Via Anguillaiese 301, 00060 Roma, Italy; salvatore.scaglione@enea.it
* Correspondence: nancy.artioli@unibs.it

Abstract

High-efficiency diesel and lean-burn engines produce lower exhaust temperatures, which can delay the activation of after-treatment catalysts such as Diesel Oxidation Catalysts (DOCs). This study explores ion beam sputtering as a post-synthesis strategy to enhance the low-temperature activity of commercial $Pt/CeO_2–ZrO_2$ catalysts. Low-energy ions (0.5–1.5 keV) were applied with controlled variations in treatment number, beam current, and exposure time to selectively generate oxygen vacancies and improve Pt dispersion. Structural and chemical effects were characterized using X-ray diffraction (XRD), BET surface area measurements, X-ray photoelectron spectroscopy (XPS) and extended X-ray absorption fine structure (EXAFS). Catalytic performance was evaluated through CO and C_3H_6 oxidation under conditions mimicking lean-burn engine exhaust. Increasing the number of ion treatments progressively lowered light-off temperatures, correlating with enhanced $Pt–Ce^{3+}$ interactions and improved surface reducibility. Variations in beam current and exposure time further modulated these surface effects, confirming the tunable nature of the approach. The results demonstrate that ion beam sputtering selectively modifies the catalyst surface without altering the bulk structure, directly linking atomic-scale modifications to improved low-temperature activity. This strategy offers a promising route to overcome delayed light-off issues in modern high-efficiency engines, providing a precise, controllable method to optimize emission control catalysts.

Keywords: ion beam sputtering; $Pt/CeO_2–ZrO_2$ catalysts; automotive emission control; light-off temperature; CO and hydrocarbon oxidation; post-synthesis surface modification

Academic Editors: Feng Wang, Xiyu Cheng and Jianhua Hu

Received: 1 October 2025
Revised: 21 October 2025
Accepted: 23 October 2025
Published: 30 October 2025

Citation: O'Donnell, R.; Maddaloni, M.; Scaglione, S.; Artioli, N. Post-Synthesis Ion Beam Sputtering of $Pt/CeO_2–ZrO_2$ Catalysts: Correlating Surface Modifications with Light-Off Performance. *Catalysts* **2025**, *15*, 1018. https://doi.org/10.3390/catal15111018

1. Introduction

Since the early 1990s, the European Commission's Thematic Strategy on Air Pollution has progressively introduced more stringent standards to reduce transport-related emissions (CO, hydrocarbons, NOx, PM, etc.), as part of a broader effort to improve air quality and, more broadly, to support the EU's long-term objective of achieving carbon neutrality by 2050, in line with ongoing research and strategies for sustainable energy and low-carbon technologies [1–4]. The transition from Euro 5 in 2009 to Euro 6/VI in 2014 marked a significant tightening of NOx emission limits for diesel engines: from 0.18 g/km (Euro 5) to 0.08 g/km (Euro 6) for light-duty vehicles and from 2.0 g/kWh (Euro V) to

0.4 g/kWh (Euro VI) for heavy-duty vehicles. This regulatory change accelerated the adoption of advanced after-treatment technologies, including Selective Catalytic Reduction (SCR), Lean NOx Traps (LNT), and Diesel Oxidation Catalysts (DOC). Building on this trajectory, the forthcoming Euro 7 regulation—scheduled to apply from 2027—further strengthens emission limits across all vehicle categories. Unlike previous standards, Euro 7 introduces a unified framework for light- and heavy-duty vehicles, expands testing conditions (e.g., real-world driving emissions over a wider temperature and lifetime range), and places stricter durability requirements on emission-control systems. These measures are expected to drive the next generation of catalyst technologies and integrated powertrain solutions [1,5,6].

Many of these catalytic converters, particularly DOCs, are based on Pt–ceria/zirconia materials, where the complementary functionalities of ceria and Pt play a pivotal role. In particular, the incorporation of ZrO_2 into CeO_2 has been widely recognized as a strategy to enhance both the structural and functional properties of ceria-based catalysts. Zirconium addition improves the thermal stability of the mixed oxide, reducing the propensity for sintering at high operating temperatures, which is critical for maintaining the dispersion of noble metal nanoparticles under harsh exhaust conditions. Moreover, the formation of CeO_2–ZrO_2 solid solutions enhances the oxygen storage capacity (OSC) of the support, a key property for dynamic oxygen buffering during rich–lean cycling, which in turn facilitates the reversible Ce^{4+}/Ce^{3+} redox transition. This increase in OSC not only improves the redox flexibility of the support but also provides a greater density of surface defects and oxygen vacancies, which act as preferential anchoring sites for Pt atoms. By stabilizing Pt species and preventing their migration or sintering, the addition of ZrO_2 effectively supports higher metal dispersion and stronger metal–support interactions, thus contributing to the overall catalytic efficiency and durability of the system [7,8]. These advantages explain why Pt–ceria/zirconia catalysts remain the benchmark for modern automotive DOCs and provide the rationale for their widespread use in emission-control applications.

The remarkable performance of ceria arises from its redox flexibility, enabled by the facile and reversible transition between Ce^{4+} and Ce^{3+}, which confers a substantial oxygen storage capacity (OSC). This dynamic oxygen buffering, facilitated by the formation of oxygen vacancies, allows ceria to repeatedly adsorb and release O^{2-}, thereby promoting the oxidation of exhaust gases under transient rich–lean conditions [9]. At the same time, Pt provides exceptionally high oxidation activity, particularly toward NOx. When combined, the oxygen-buffering capacity of ceria-based supports and the intrinsic oxidation activity of Pt create a synergistic system that underpins the effectiveness of modern automotive emission-control catalysts [10].

A critical performance parameter of Diesel Oxidation Catalysts (DOCs) is the so-called light-off temperature, defined as the temperature at which catalytic reactions begin and, in practice, as the catalyst inlet temperature at which 50% of a given pollutant species is converted. Below this threshold, catalytic activity is minimal, while above it, the reaction rate increases exponentially with temperature. Achieving rapid light-off is therefore essential to ensure efficient pollutant conversion, particularly during the cold-start phase, when emissions are most severe [11,12].

The challenge, however, lies in the fact that modern diesel and lean-burn engines are designed for high thermal efficiency, which inherently results in lower exhaust gas temperatures. While this trend improves fuel economy and reduces CO_2 emissions, it simultaneously delays—or even prevents—after-treatment systems from reaching their activation threshold under certain operating conditions [13,14]. Technologies such as DOCs, Diesel Particulate Filters (DPFs), Lean NOx Traps (LNTs), and Selective Catalytic Reduction (SCR) all depend on surpassing their respective light-off temperatures to function effectively.

During cold-start and low-load operation, however, the exhaust often remains below these critical temperatures, leaving the catalysts largely inactive and causing substantial emissions of NOx and particulate matter [15].

This limitation has become particularly critical under Euro 6/VI regulations, which enforce stringent emission limits not only under controlled laboratory tests but also in real driving conditions. As a result, significant research efforts are currently directed toward lowering the light-off temperature of catalytic materials or developing strategies to accelerate catalyst heating, thereby ensuring compliance with these demanding standards while preserving engine efficiency.

In this context, interface engineering using ion beam techniques has emerged as a powerful approach to tailor catalytic properties at the atomic scale, enabling precise structural modifications that can directly influence the catalyst's light-off temperature [16]. Among the different strategies, ion beam sputtering has attracted growing interest as a versatile tool to modify the nanoscale surface structure of advanced catalytic materials, particularly in the development of automotive after-treatment systems [17,18]. The use of low-energy accelerated ions (0.5–10 keV) enables controlled interactions with surface atoms of the catalyst without penetrating deeply into the bulk [19]. This process results in a "non-reactive removal" of atoms—commonly referred to as sputtering—where surface atoms are displaced without undergoing chemical reactions with the incident ions [20].

Beyond these general advantages, the selectivity of ion-beam sputtering can be particularly beneficial in mixed Pt–CeO_2 oxides. In this case, oxygen can be sputtered more readily than either Pt or ceria, thereby generating oxygen vacancies (V_O). These defects increase the concentration of Ce^{3+} in the structure, making the surface more reducible and receptive toward Pt, ultimately leading to stronger Pt–support interactions [21,22]. Several studies in the literature [22–24] have demonstrated that the creation of surface defects, including oxygen vacancies (V_O), can act as "energetic traps" for Pt atoms. Owing to the reducing nature of Ce^{3+}, the oxidation state of Pt can be modulated, which stabilizes Pt atoms on the surface, prevents their migration and sintering, and thus enhances their dispersion across the support [25].

Nevertheless, as with any emerging technique, some critical issues have also been raised. Wolf et al. [26] pointed out a potential limitation of ion sputtering and ion implantation for metal deposition: the reduction in the surface-active area caused by atoms being buried beneath the substrate. This observation underscores the need to carefully optimize ion beam parameters in order to exploit the advantages of the technique without compromising catalytic efficiency.

Yet, these challenges also highlight an underexplored opportunity. Only a limited number of studies have investigated the use of ion beams as a post-synthesis modification strategy, and here ion beam sputtering offers a distinctive advantage over other ion beam methods: it allows selective tuning of surface properties while leaving the bulk structure largely unaffected. This unique capability opens the way to targeted improvements in catalytic activity and stability. For example, Machida et al. [27] demonstrated the potential of post-synthesis ion implantation by employing O^+ and N^+ ions to modify noble metal catalysts supported on Al_2O_3 for methane oxidation, thereby providing experimental evidence of the effectiveness of ion-based surface processing.

In this study, we explore ion beam sputtering as a post-synthesis modification of commercial Pt/CeO_2–ZrO_2 catalysts for automotive emission control. Using low-energy ions, the surface is selectively modified to generate oxygen vacancies and enhance Pt dispersion, promoting a strong synergy between Pt and the redox-active ceria. Surface changes were characterized by XPS and EXAFS and complemented with SRIM simulations to elucidate the structural effects induced by sputtering.

Catalytic performance was evaluated via CO and hydrocarbon oxidation under conditions mimicking lean-burn engine exhaust. The enhanced interaction between Pt and Ce^{3+}–rich sites facilitates pollutant activation at lower temperatures, effectively addressing the delayed light-off issue associated with modern high-efficiency engines.

This work demonstrates that ion beam sputtering is an effective post-treatment strategy to tune catalyst surfaces, directly linking atomic-scale modifications to improved low-temperature activity in real-world emission control applications.

2. Results and Discussion

The structural stability of the $Pt/Ce_{0.5}Zr_{0.5}O_2$ catalyst after ion beam treatment was first assessed by X-ray diffraction (XRD) (Figure 1). All irradiated samples exhibited diffraction patterns consistent with the cubic fluorite-type $Ce_{0.5}Zr_{0.5}O_2$ solid solution, showing reflections at $2\theta = 29.2°$, $33.8°$, $48.6°$, $57.1°$, $60.5°$, $71.1°$, and $78.7°$, corresponding to the (111), (200), (220), (311), (222), (400), and (331) planes, respectively [28]. No appreciable changes in peak positions, intensities, or widths were observed, even in samples exposed to the most severe bombardment conditions (Pt1.5(16 × 4)), which accumulated 64 irradiation cycles. These results clearly indicate that ion beam sputtering does not compromise the long-range crystallinity of the $Ce_{0.5}Zr_{0.5}O_2$ lattice, supporting the hypothesis that structural modifications are confined to the near-surface region.

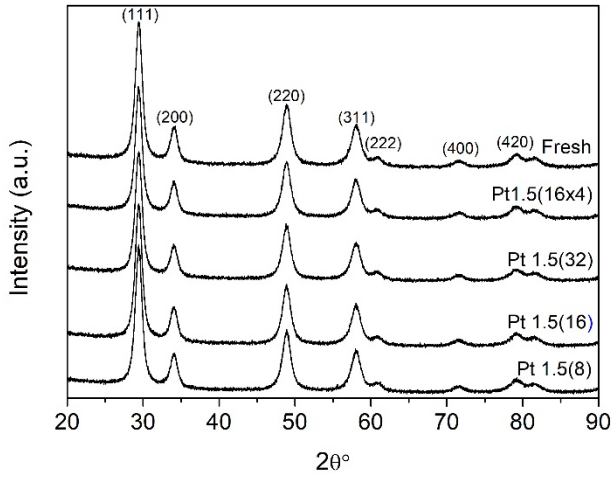

Figure 1. XRD patterns of the fresh 1 wt.% $Pt/Ce_{0.5}Zr_{0.5}O_2$ catalyst compared with those of the ion-bombarded samples. The number of irradiation treatments ranged from 8 cycles for Pt1.5(8) to 64 cumulative cycles for Pt1.5(16 × 4).

BET N_2 physisorption measurements further corroborated the bulk stability of the catalysts (Table 1). The fresh sample displayed a specific surface area of 88.2 $m^2\ g^{-1}$, and all treated materials retained values in the range of 86.7–89.9 $m^2\ g^{-1}$, well within the experimental error. This invariance confirms that ion bombardment does not affect textural properties such as porosity or accessible surface area. Together, the XRD and BET data establish that ion sputtering introduces subtle modifications localized at the surface without altering the overall framework of the mixed-oxide support.

Importantly, no Pt reflections were detected in any of the XRD patterns, as expected given the low noble metal loading (1 wt.%) and the high dispersion of Pt species, which lie below the detection limit of conventional diffractometry. Although XRD alone cannot provide direct evidence of enhanced dispersion upon ion treatment, complementary spectroscopic and structural data—including the downward shift of the PtO_x reduction peak in TPR, the decreased accessible Pt signal in XPS, and the reduction of surface Pt measured by XRF—indicate stronger metal–support interaction and redistribution of Pt

species. This interpretation is further supported by our previous study on N^+-irradiated $Pt/Ce_{0.68}Zr_{0.32}O_2$ [16], where high-resolution TEM revealed a finer Pt particle distribution and partial embedding into a defect-rich oxide surface, providing direct microscopic confirmation that ion irradiation can stabilize highly dispersed Pt species. Together, these observations suggest that the current Ar^+ treatment induces similar defect-mediated redistribution and anchoring of Pt nanoparticles. This observation is also consistent with prior reports on Pt/ceria–zirconia materials [29], in which Pt is generally present as highly dispersed oxidic clusters or atomically anchored species rather than crystalline nanoparticles detectable by XRD. The combination of these findings strengthens the conclusion that the observed decrease in surface Pt measured by XRF does not imply detrimental loss of catalytic functionality, but rather a reorganization toward more active Pt sites.

Table 1. Ion beam treatment parameters applied to the post-synthesis modification of the fresh $Pt/Ce_{0.5}Zr_{0.5}O_2$ catalyst (1 wt.% Pt).

Sample	Energy keV	Current (mA)	No. of Treatments	Duration of Each Treatment (mins)	BET Surface Area (m^2 g^{-1})
Fresh	-	-	-	-	88.2
Pt1.5(16 × 4)	1.5	20	16 × 4 100 mg batches	15	87.3
Pt1.5(32)	1.5	20	32	15	86.8
Pt1.5(16)	1.5	20	16	15	86.7
Pt1.5(8)	1.5	20	8	15	89.7
Pt1.2(16)	1.2	20	16	15	88.2
Pt1.5(8)-10	1.5	10	8	15	87.2
Pt1.5(16)-2	1.5	20	16	2	89.9

While the bulk remained unchanged, temperature-programmed reduction (TPR) experiments revealed significant modifications in redox properties induced by ion sputtering (Figure 2). The fresh catalyst exhibited a well-defined H_2 consumption peak centered at ~415 K, attributable to the reduction of surface PtO_x species [30,31]. Given that the reduction of $Ce_{0.5}Zr_{0.5}O_2$ occurs above 773 K, no support-related features were detected in the investigated temperature range. Upon ion bombardment, this reduction peak progressively shifted toward lower temperatures, with onsets as low as 395 K. This indicates that Pt species became more easily reducible after irradiation, suggesting a modified electronic environment and stronger coupling with the support. Interestingly, the integrated H_2 uptake decreased systematically from 61.3 μmol g^{-1} in the fresh sample to 41–46 μmol g^{-1} in treated catalysts. This reduced hydrogen consumption is consistent with partial removal or redistribution of Pt during sputtering. Indeed, XRF analysis confirmed a measurable decrease in Pt loading at the surface after irradiation. Thus, although a fraction of Pt is lost, the remaining species become more reducible and more strongly interacting with the modified support. These TPR results are fully consistent with our recent findings on N^+-irradiated $Pt/Ce_{0.68}Zr_{0.32}O_2$ catalysts [16], where a comparable downward shift (~180 K) of the PtO_x reduction peak was observed. In that study, operando FTIR spectra in the νOH region provided direct spectroscopic evidence of oxygen vacancy formation, confirming that ion irradiation promotes selective oxygen removal and defect generation within the ceria–zirconia lattice. The parallel behavior observed here under Ar^+ sputtering further supports the conclusion that the enhanced reducibility originates from vacancy-mediated activation of the Pt–CeO_2 interfacial redox couple, rather than from a simple weakening of metal–support interactions.

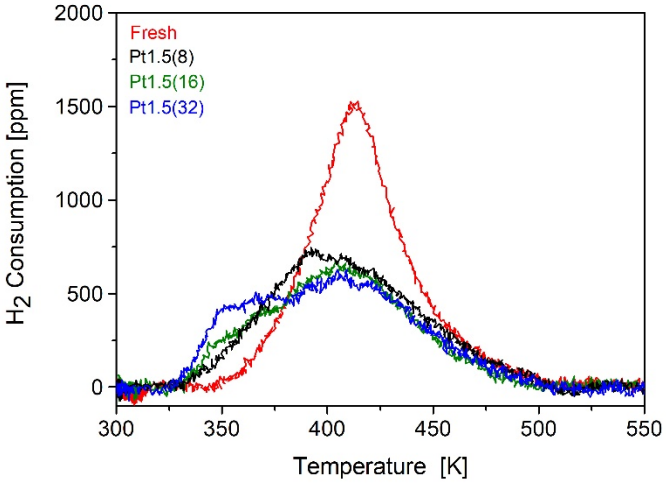

Figure 2. TPR profiles of the fresh 1 wt.% $Pt/Ce_{0.5}Zr_{0.5}O_2$ catalyst compared with those of the ion-bombarded samples, treated with increasing numbers of irradiation cycles ranging from 8 [Pt1.5(8)] to 32 [Pt1.5(32)].

X-ray photoelectron spectroscopy (XPS) provided further evidence of these changes (Figure 3). The Pt 4f spectra (Figure 3a) of all samples revealed predominantly oxidic Pt species, with Pt^{2+} as the dominant component. However, in the case of prolonged irradiation (Pt1.5(32)), a small fraction of metallic Pt^0 emerged, suggesting that extensive sputtering can locally alter the oxidation state of Pt. Moreover, overall Pt content (Figure 3b) decreased with increasing irradiation cycles, consistent with either partial Pt removal during sputtering or the formation of oxidic overlayers that attenuate the XPS signal [30]. More revealing were the modifications in the Ce 3d region (Figure 3c). Curve fitting of the multiplets, following the methodology of Romeo et al. [32], indicated a progressive increase in the fraction of Ce^{3+} with increasing ion exposure (Figure 3d). This trend aligns closely with the generation of oxygen vacancy (V_O), consistent with the expected preferential sputtering of oxygen atoms from the ceria lattice. A similar evolution of the Ce 3d spectra was also observed in our previously published work on N^+-irradiated $Pt/Ce_{0.68}Zr_{0.32}O_2$, where an increased Ce^{3+} contribution was attributed to partial lattice reduction and the formation of Ce^{3+}–V_O pairs at the surface. These defect sites were shown to act as preferential anchoring centers for Pt species, facilitating stronger metal–support coupling and enhancing interfacial redox flexibility. This interpretation is in excellent agreement with the mechanism proposed by Clark et al. [21], who reported that ion bombardment in Pt/CeO_2 systems generates surface oxygen vacancies that strengthen interfacial interactions. Therefore, the consistent evolution of both TPR and XPS features in our Ar^+- and N^+-irradiated catalysts strongly supports the conclusion that ion-beam-induced defect formation represents a general and reproducible mechanism to modulate the electronic and redox behavior of ceria–zirconia-supported systems. The formation of Ce^{3+}–V_O pairs is known to increase the reducibility of ceria and to provide anchoring sites for noble metals, thereby strengthening metal–support interactions. Such defect engineering has been widely reported as a key factor in enhancing the catalytic activity and stability of ceria-based materials [21,33,34].

The preferential generation of oxygen vacancies was further corroborated by SRIM-2013 simulations (Figure 4). At ion energies of 1.5 keV, the simulations predict that nearly 78% of sputtered atoms correspond to oxygen, a value significantly higher than the 66.7% expected from the stoichiometry of $Ce_{0.7}Zr_{0.3}O_2$. This selective oxygen removal, compared with only ~16–17% Ce and ~5% Zr, explains the enrichment in Ce^{3+} observed by XPS and the enhanced reducibility evidenced in TPR profiles. Importantly, the simulations

confirm that oxygen depletion is not random but preferential, directly linking ion bombardment with the creation of catalytically relevant surface defects. This preferential vacancy formation provides the structural basis for the observed stabilization of Pt species and the enhanced interfacial redox activity, consistent with mechanisms involving hydrogen spillover and Ce^{3+}–V_O pairing described in Clark et al. [21] and supported by our previous N^+-irradiation study [16].

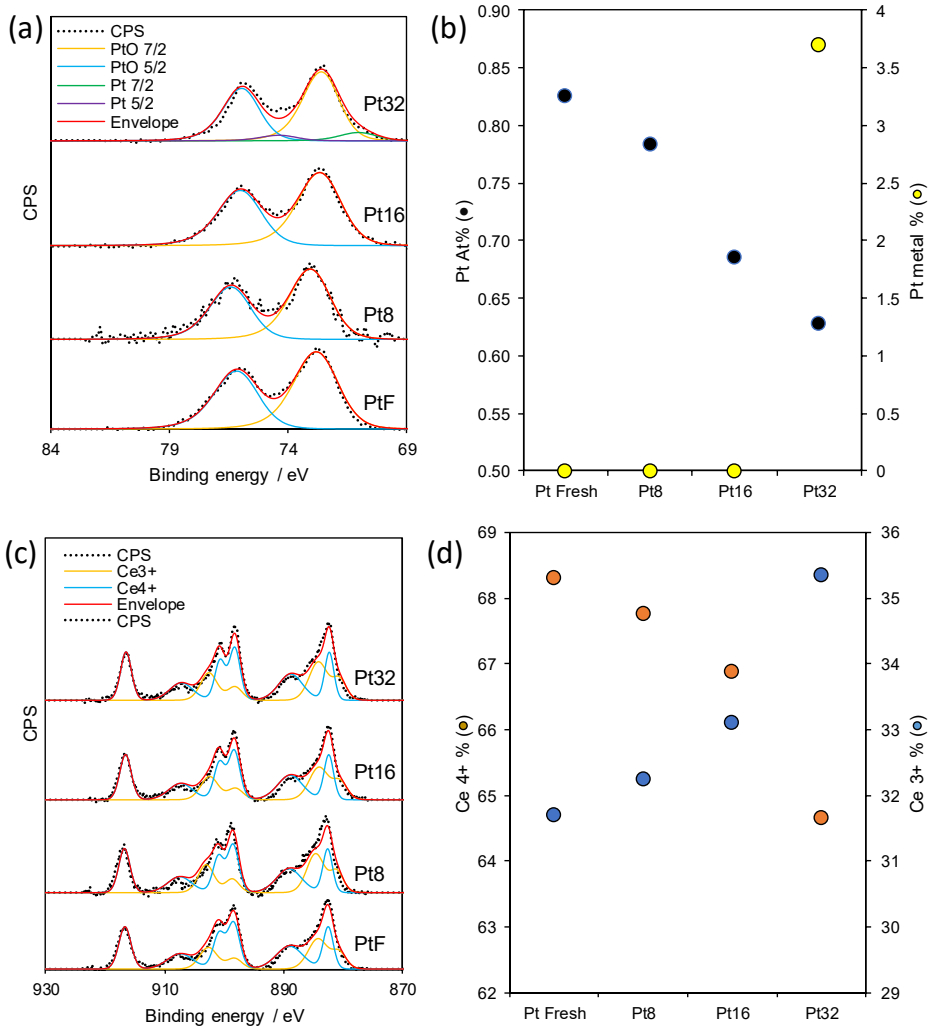

Figure 3. (**a**) Pt 4f XP spectra, (**b**) At% of Pt and deconvolution quantification of Pt metal content, (**c**) Ce 4f XP spectra, and (**d**) quantification of Ce^{3+} and Ce^{4+} in Pt Fresh, Pt8, Pt16, and Pt32 materials.

To confirm that these modifications were confined to ceria, the Zr 3d spectra were also examined (Figure 5).

Across all samples, zirconium remained fully oxidized as Zr^{4+}, unaffected by irradiation. This observation reinforces that ion sputtering selectively targets oxygen atoms in the ceria component while leaving the zirconia lattice chemically unaltered, in agreement with its lower sputtering yield.

The catalytic consequences of these surface modifications were evaluated under simulated lean-burn exhaust conditions. CO and C_3H_6 light-off curves are presented in Figure 6A and Figure 6B, respectively. The fresh catalyst exhibited T_{50} values of 513 K (CO) and 546 K (C_3H_6). Upon ion treatment, both light-off temperatures decreased progressively with the severity of irradiation. The most extensively bombarded catalyst, Pt1.5(16 × 4), achieved T_{50} values of 500 K for CO and 524 K for C_3H_6, representing improvements of 13 K and 22 K, respectively. Although modest in absolute numbers, these shifts are

highly relevant in the context of automotive emission control, where lowering the light-off temperature by even a few tens of degrees can markedly reduce cold-start emissions. The correlation between increased Ce^{3+}–V_O populations and decreased light-off temperatures supports the mechanistic hypothesis that these vacancies enhance Pt–ceria interfacial redox synergy, promoting more efficient CO and hydrocarbon oxidation.

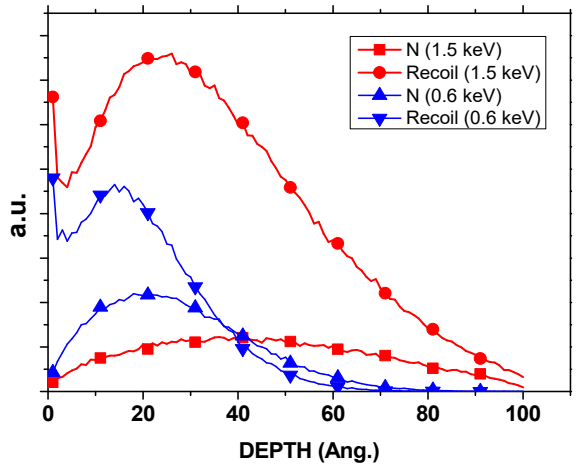

Figure 4. SRIM depth distribution profiles of incident N^+ ions and recoiled atoms within a 10 nm $Ce_{0.7}Zr_{0.3}O_2$ layer for two ion energies, 1.5 keV and 0.6 keV.

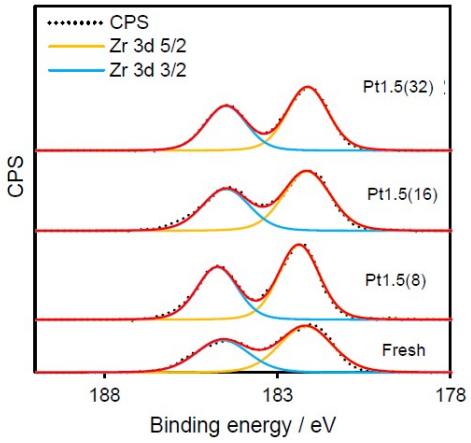

Figure 5. Zr 3d XPS spectra of Pt fresh, Pt8, Pt16, and Pt32 Pt/CeO_2–ZrO_2 catalysts after ion beam treatment. Red line is the fitted profile of Zr 3d XPS spectra.

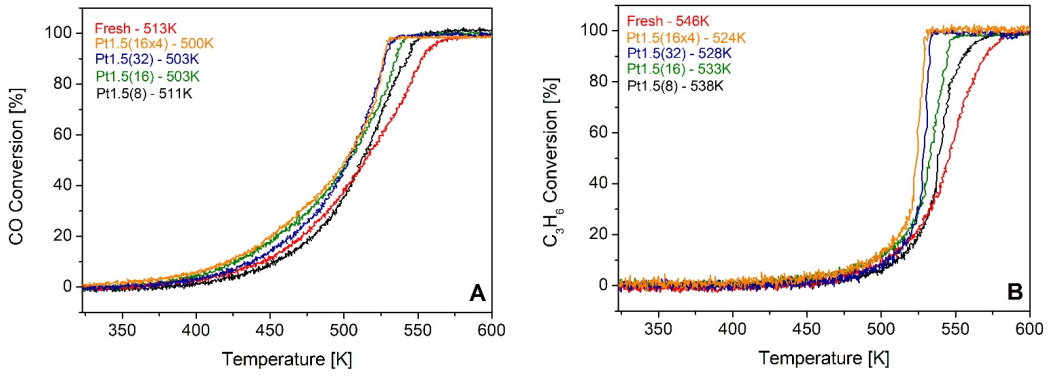

Figure 6. CO (**A**) and C_3H_6 (**B**) light-off curves obtained over a fresh Pt 1 wt.% $Ce_{0.5}Zr_{0.5}O_2$ catalyst compared to those of the samples that had been modified by ion bombardment. The number of treatments given to the samples ranges from 8 (Pt1.5(8)) to 64 (Pt1.5(16 × 4)).

The enhanced performance directly correlates with the increase in Ce^{3+} concentration and the improved reducibility observed by XPS and TPR, confirming that oxygen vacancies generated by sputtering enhance the activation of CO and hydrocarbons at lower temperatures. Interestingly, CH_4 oxidation remained largely unaffected by ion treatment, with T_{50} values unchanged relative to the fresh catalyst. This behavior is consistent with the inherently higher activation barrier for methane oxidation [27], which requires more drastic modifications (e.g., higher Pt loadings or different promoters) to be significantly improved.

To gain mechanistic insight, the influence of beam energy, current, and exposure time was systematically investigated. Variation of the accelerating voltage between 1.2 and 1.5 keV (Figure 7) produced essentially identical CO and C_3H_6 light-off temperatures, indicating that within this narrow energy window, the penetration depth of the ions does not play a dominant role. Similarly, reducing the beam current from 20 to 10 mA (Pt1.5(8) vs. Pt1.5(8)-10, Figure 8) resulted in nearly overlapping light-off curves, suggesting that moderate variations in ion flux density are not decisive for the catalytic outcome.

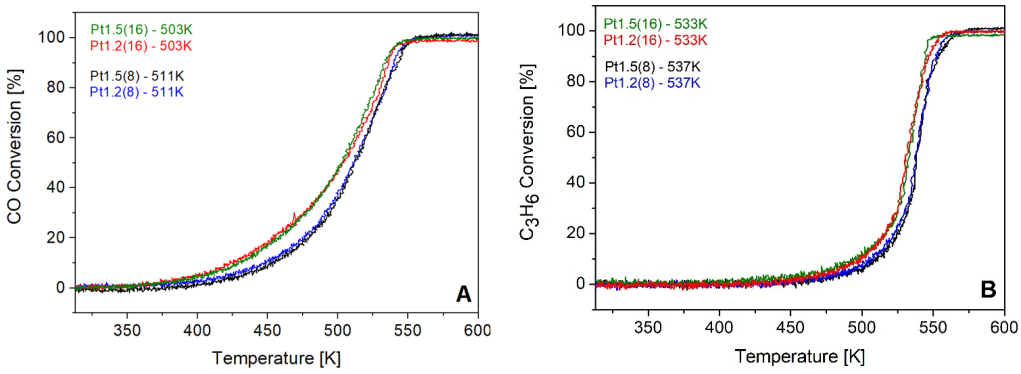

Figure 7. CO (**A**) and C_3H_6 (**B**) light-off curves over fresh Pt 1 wt.% $Ce_{0.5}Zr_{0.5}O_2$ catalyst compared with samples treated with an ion beam of 1.2 keV and 1.5 keV.

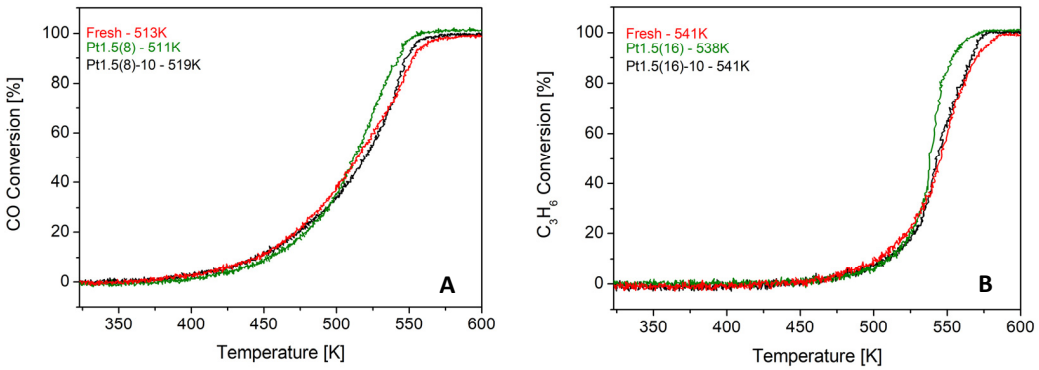

Figure 8. Comparison of light-off curves for samples treated with eight ion beam sputtering cycles at 1.5 keV and a current of 10 mA Pt1.5(8)-10 (**A**) and the sample treated under the same conditions with 20 mA (Pt1.5(8)) (**B**).

These experimental findings are consistent with the SRIM depth distribution profiles (Figure 9), which show that at 1.5 keV, atomic mixing extends throughout an entire 10 nm grain, whereas at 0.6 keV, the effect is largely confined to the outermost surface layers. Since catalytic activity is governed by near-surface phenomena, both energies were sufficient to induce the oxygen vacancy formation necessary for activity enhancement, explaining why small variations in beam energy within the tested range did not produce significant differences in light-off curves.

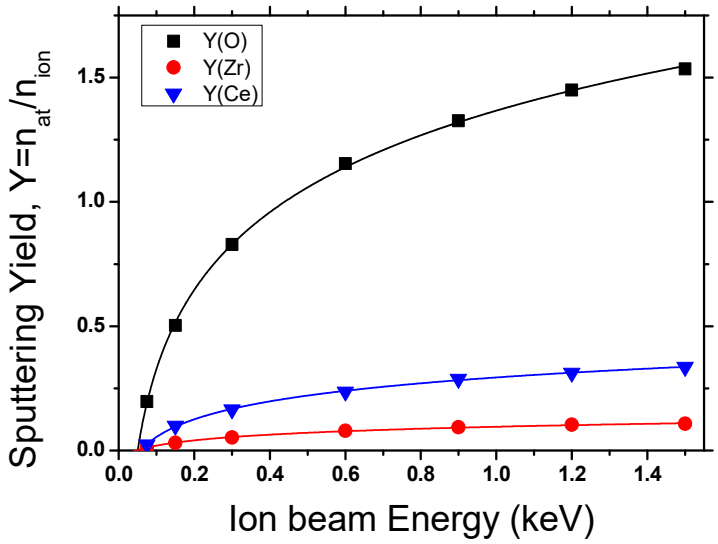

Figure 9. Correlation between SRIM simulations and experimental data, evidencing preferential oxygen sputtering and the stabilization of Ce^{3+}–V_O sites as the key factor behind the observed catalytic enhancement.

By contrast, the duration of each treatment emerged as a critical factor. When 16 treatments were applied with standard 15-min exposures (Pt1.5(16)), significant improvements were observed (CO T_{50} = 502 K, C_3H_6 T_{50} = 532 K). However, shortening the exposure to only 2 min per cycle (Pt1.5(16)-2) almost completely suppressed the beneficial effect, with light-off values (CO T_{50} = 514 K, C_3H_6 T_{50} = 546 K) close to the fresh catalyst (Figure 10). These findings confirm that a sufficient ion–surface interaction time is required to generate a meaningful concentration of oxygen vacancies and to stabilize Pt at the interface.

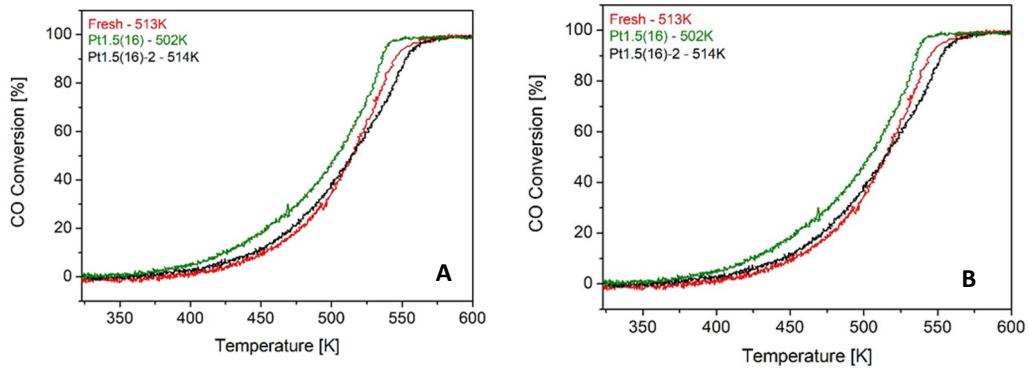

Figure 10. CO (**A**) and C3H6 (**B**) light-off curves over fresh Pt 1 wt.% $Ce_{0.5}Zr_{0.5}O_2$ catalyst compared with Pt1.5(16) and Pt1.5(16)-2, which had been exposed to the ion beam for 15 min and 2 min, respectively, during each treatment.

Taken together, these results establish a clear structure–activity correlation. Ion beam sputtering selectively removes oxygen atoms from the ceria lattice, generating oxygen vacancies and increasing the Ce^{3+} fraction. These defects act as anchoring sites for Pt, preventing migration and sintering, while simultaneously enhancing the reducibility and oxygen mobility of the support. The resulting Pt–Ce^{3+} interfacial synergy lowers the activation barrier for CO and hydrocarbon oxidation, leading to earlier light-off under lean-burn conditions. The fact that bulk crystallinity, surface area, and zirconia oxidation state remain unaffected highlights the surface-confined and tunable nature of this modification.

The simulations also provided quantitative estimates consistent with the experimental mass loss of treated samples, confirming that oxygen removal dominates the sputtering

process under the tested conditions. The preferential sputtering of oxygen promotes the stabilization of Ce^{3+}–V_O sites, which act as anchoring points for Pt species and enhance Pt–ceria interfacial synergy. Together with the experimental evidence, the simulation results reinforce the conclusion that catalytic improvement arises from controlled, surface-confined oxygen depletion rather than bulk structural changes.

Moreover, the parameter study demonstrates that catalytic improvements are controlled by the extent of surface exposure—dictated by the number and duration of treatments—rather than by small variations in beam energy or current. This confirms that the decisive factor is the accumulation of sufficient surface defects rather than changes in penetration depth or ion flux density.

The present findings align with previous literature on [35], but extend this knowledge to a commercially relevant Pt/Ce–Zr system under realistic lean-burn exhaust conditions. By demonstrating reproducible and controllable reductions in light-off temperature, ion beam sputtering emerges as a promising post-synthesis strategy to fine-tune the surface chemistry of existing catalysts. Crucially, this approach provides a scalable means of addressing the persistent challenge of cold-start emissions in high-efficiency diesel and lean-burn engines, offering a pathway towards the development of next-generation emission-control systems.

3. Materials and Methods

3.1. Catalyst Preparation

A commercial $Pt/Ce_{0.5}Zr_{0.5}O_2$ catalyst (1 wt.% Pt, "Fresh"), commercially supplied by Rhodia (now Solvay, Brussels, Belgium), with detailed characterization in [36], was subjected to ion beam irradiation under controlled conditions. A 600 mg sample was placed in a 2 cm^2 holder and irradiated in a vacuum chamber using a Kaufman ion source (monoenergetic beam, 90° incidence). To ensure uniform exposure, the catalyst was periodically mixed between irradiation cycles to present fresh surface areas to the beam. The irradiation parameters—ion energy, beam current, exposure time, and number of treatment cycles—were systematically varied, as summarized in Table 1. The resulting samples were designated as PtX(Y), where X corresponds to the applied ion energy (keV) and Y to the number of irradiation treatments.

Specifically, the notation Pt1.5(16 × 4) indicates that four independent batches of approximately 100 mg each were irradiated under identical conditions (beam current 20 mA, ion energy 1.5 keV). Each batch underwent 16 consecutive irradiation runs of 15 min, ensuring reproducibility and providing sufficient treated material for subsequent analyses. Representative examples include Pt1.5(16 × 4), Pt1.5(8)-10, and Pt1.5(16)-2.

3.2. Catalytic Testing

Catalytic performance was assessed under conditions representative of lean-burn engine exhaust. Light-off experiments were conducted to determine the T_{50} values for CO and C_3H_6 oxidation. Tests were carried out in a fixed-bed quartz microreactor (inner diameter: 0.6 cm; length: 30 cm) loaded with 0.1 g of catalyst and housed in a tubular furnace. Reactor temperature was regulated using a Eurotherm (Ashburn, VA, USA) PID controller and monitored by a K-type thermocouple positioned at the center of the catalyst bed. The feed gas composition was maintained at a total flow rate corresponding to 16.7 $cm^3\ g^{-1}\ s^{-1}$, consisting of 10% O_2, 4.5% H_2O, 2000 ppm CO, 2000 ppm CH_4, 2000 ppm C_3H_6, and 200 ppm NO, with Ar as the balance gas. The reactor temperature was ramped from 313 to 773 K at a heating rate of 0.083 $K\ s^{-1}$. Product gases were continuously analyzed using a Pfeiffer OmniStar (Asslar, Germany) quadrupole mass spectrometer. To ensure

reproducibility, three consecutive light-off cycles were performed; catalytic data presented herein correspond to the third cycle.

To complement the experimental characterization, simulations of N^+ ion bombardment were performed using SRIM-2013 (Stopping and Range of Ions in Matter—James F. Ziegler, Newtown, PA, USA). A $Ce_{0.7}Zr_{0.3}O_2$ lattice model was used to approximate the mixed oxide support composition. Ion energies of 0.6 and 1.5 keV were selected to reproduce the experimental conditions applied during ion beam sputtering, with normal incidence (90°) and a fluence consistent with the number of treatment cycles reported in Table 1. The simulations provided depth profiles of implanted ions and recoil distributions, as well as sputtering yields for O, Ce, and Zr atoms. These data were used to quantify the preferential removal of oxygen compared to the cations, to estimate the degree of atomic mixing within ~10 nm grains, and to rationalize the experimental findings of enhanced reducibility and increased Ce^{3+} concentration.

3.3. Material Characterization

The structural and physicochemical properties of the catalysts were investigated using a combination of ex situ techniques. X-ray diffraction (XRD) patterns were collected on a PANalytical (Malvern, UK) X'Pert Pro diffractometer equipped with Cu Kα radiation (40 kV, 40 mA), scanning over the 2θ range of 15–90° with a step size of 0.017°, with samples mounted on quartz zero-background holders. Textural properties, including specific surface area, pore volume, and pore size distribution, were determined by N_2 adsorption–desorption at 77 K using a Micromeritics (Norcross, GA, USA) ASAP 2010 instrument after sample degassing at 393 K under vacuum for 24 h. Platinum loading was quantified by energy-dispersive X-ray fluorescence (EDXRF) using a Rigaku (Tokyo, Japan) NEX QC+ QuantEZ analyzer. Temperature-programmed reduction (TPR) experiments were conducted following pretreatment in 3% O_2 (ambient temperature to 773 K, 5 K min^{-1}, 90 min isothermal hold), cooling under Ar, and subsequent exposure to 4000 ppm H_2 in Ar at a flow rate of 16.7 cm^3 g^{-1} s^{-1}. X-ray photoelectron spectroscopy (XPS) was performed on a Kratos Axis SUPRA instrument (Kratos Analytical Ltd., Manchester, UK) with Al Kα excitation (1486.69 eV, 12 mA, 15 kV, 700 × 300 μm analysis area). High-resolution spectra were acquired at a pass energy of 20 eV with 0.1 eV step size and 60 s acquisition time, employing an electron flood gun for charge compensation. Binding energies were calibrated to the C 1s peak at 284.8 eV, and data analysis was conducted using CasaXPS (v2.3.19PR1.0). Extended X-ray absorption fine structure (EXAFS) spectroscopy was performed at the Pt L_3-edge at the Diamond Light Source (UK), with first-shell fitting applied to determine Pt–O coordination environments.

4. Conclusions

This work demonstrates the effectiveness of ion beam sputtering as a post-synthesis surface engineering strategy for $Pt/Ce_{0.5}Zr_{0.5}O_2$ catalysts employed in automotive emission control. Comprehensive structural and spectroscopic analyses confirmed that low-energy ion irradiation selectively modified the near-surface region by generating oxygen vacancies and increasing the Ce^{3+} fraction, while preserving the bulk crystallinity and textural properties of the support. These surface modifications enhanced Pt–ceria interactions and improved redox behavior, as evidenced by shifts in TPR profiles and XPS analysis. Catalytic testing under lean-burn exhaust conditions revealed consistent reductions in light-off temperatures for CO and C_3H_6 oxidation, with the extent of improvement directly correlated to the cumulative ion exposure (number and duration of treatments). In contrast, variations in beam energy and current within the investigated ranges had negligible effects on performance, underscoring that surface activation is primarily governed by the degree

of exposure rather than the specific irradiation parameters. Overall, the findings establish ion beam sputtering as a reproducible and controllable approach to fine-tune catalyst surfaces at the atomic scale. By directly linking surface defect engineering to measurable enhancements in low-temperature activity, this study highlights the potential of ion beam processing to address the persistent challenge of cold-start emissions in high-efficiency diesel and lean-burn engines. The strategy provides a precise, non-synthetic route to optimize existing commercial catalysts, offering new opportunities for the design of next-generation emission-control materials compliant with forthcoming Euro 7 regulations.

Author Contributions: R.O.: Methodology, formal analysis, investigation, data curation, visualization, M.M.: Methodology, formal analysis, resources, data curation, writing—original draft preparation, visualization, S.S.: formal analysis, data curation, visualization, N.A.: Conceptualization, Methodology, validation, resources, data curation, writing—original draft preparation, project administration, supervision. All authors have read and agreed to the published version of the manuscript.

Funding: This research received no external funding.

Data Availability Statement: The original contributions presented in this study article. Further inquiries can be directed to the corresponding author.

Acknowledgments: The authors gratefully acknowledge Mark Isaac for his valuable assistance in acquiring the EXAFS data.

Conflicts of Interest: The authors declare no conflicts of interest.

Abbreviations

The following abbreviations are used in this manuscript:

BET	Brunauer–Emmett–Teller (surface area measurement)
DPF	Diesel Particulate Filter
DOC	Diesel Oxidation Catalyst
EXAFS	Extended X-ray Absorption Fine Structure
HC	Hydrocarbons
LNT	Lean NOx Trap
OSC	Oxygen Storage Capacity
SCR	Selective Catalytic Reduction
SRIM	Stopping and Range of Ions in Matter
TPR	Temperature-Programmed Reduction
XPS	X-ray Photoelectron Spectroscopy
XRD	X-ray Diffraction
XRF	X-ray Fluorescence
V_O	Oxygen vacancy
PID	Proportional–Integral–Derivative (temperature controller)

References

1. ICCT. *A Technical Summary of Euro 6/VI Vehicle Emission Standards*; International Council for Clean Transportation: Washington, DC, USA, 2016.
2. Maddaloni, M.; Marchionni, M.; Abbá, A.; Mascia, M.; Tola, V.; Carpanese, M.P.; Bertanza, G.; Artioli, N. Exploring the Viability of Utilizing Treated Wastewater as a Sustainable Water Resource for Green Hydrogen Generation Using Solid Oxide Electrolysis Cells (SOECs). *Water* **2023**, *15*, 2569. [CrossRef]
3. La Corte, D.; Maddaloni, M.; Vahidzadeh, R.; Domini, M.; Bertanza, G.; Ansari, S.U.; Marchionni, M.; Tola, V.; Nancy, N.A. Recovered Ammonia as a Sustainable Energy Carrier: Innovations in Recovery, Combustion, and Fuel Cells. *Energies* **2025**, *18*, 508. [CrossRef]
4. Huang, S.; Shen, J.; Wu, Y.; Li, X.; Ma, Y.; Xie, Y.; Yu, C.; Zhang, Y.; Zhang, J. $Bi_2O_2CO_3$ Co-Catalyst Modification BiOBr Driving Efficient Photoreduction CO_2. *Colloids Surf. A Physicochem. Eng. Asp.* **2025**, *725*, 137731. [CrossRef]

5. Lietti, L.; Righini, L.; Castoldi, L.; Artioli, N.; Forzatti, P. Labeled ^{15}NO Study on N_2 and N_2O Formation over Pt-Ba/Al_2O_3 NSR Catalysts. *Top. Catal.* **2013**, *56*, 7–13. [CrossRef]
6. Maddaloni, M.; Centeno-Pedrazo, A.; Avanzi, S.; Mazumdar, N.J.; Manyar, H.; Artioli, N. Novel Ionic Liquid Synthesis of Bimetallic Fe–Ru Catalysts for the Direct Hydrogenation of CO_2 to Short Chain Hydrocarbons. *Catalysts* **2023**, *13*, 1499. [CrossRef]
7. Di Monte, R.; Kašpar, J. Heterogeneous Environmental Catalysis—A Gentle Art: CeO_2-ZrO_2 Mixed Oxides as a Case History. *Catal. Today* **2005**, *100*, 27–35. [CrossRef]
8. Montini, T.; Melchionna, M.; Monai, M.; Fornasiero, P. Fundamentals and Catalytic Applications of CeO_2-Based Materials. *Chem. Rev.* **2016**, *116*, 5987–6041. [CrossRef]
9. O'Donnell, R.; Ralphs, K.; Grolleau, M.; Manyar, H.; Artioli, N. Doping Manganese Oxides with Ceria and Ceria Zirconia Using a One-Pot Sol–Gel Method for Low Temperature Diesel Oxidation Catalysts. *Top. Catal.* **2020**, *63*, 351–362. [CrossRef]
10. Karre, A.V.; Garlapalli, R.K.; Jena, A.; Tripathi, N. State of the Art Developments in Oxidation Performance and Deactivation of Diesel Oxidation Catalyst (DOC). *Catal. Commun.* **2023**, *179*, 106682. [CrossRef]
11. Lafyatis, D.S.; Ansell, G.P.; Bennett, S.C.; Frost, J.C.; Millington, P.J.; Rajaram, R.R.; Walker, A.P.; Ballinger, T.H. Ambient Temperature Light-off for Automobile Emission Control. *Appl. Catal. B Environ.* **1998**, *18*, 123–135. [CrossRef]
12. Coise Duprat, F. Light-off Curve of Catalytic Reaction and Kinetics. *Chem. Eng. Sci.* **2002**, *57*, 901–911. [CrossRef]
13. Li, T.; Zhao, P.; He, H.; Wang, C.; Zhang, H.; Chen, Z.; Chen, H. Dual-Fuel Dual-Direct Injection: An Efficient and Clean Combustion Technology for Diesel Engines. *J. Energy Inst.* **2025**, *119*, 102006. [CrossRef]
14. Dardiotis, C.; Martini, G.; Marotta, A.; Manfredi, U. Low-Temperature Cold-Start Gaseous Emissions of Late Technology Passenger Cars. *Appl. Energy* **2013**, *111*, 468–478. [CrossRef]
15. Ye, S.; Yap, Y.H.; Kolaczkowski, S.T.; Robinson, K.; Lukyanov, D. Catalyst "light-off" Experiments on a Diesel Oxidation Catalyst Connected to a Diesel Engine-Methodology and Techniques. *Chem. Eng. Res. Des.* **2012**, *90*, 834–845. [CrossRef]
16. Solt, H.; Maddaloni, M.; Bazin, P.; Aureau, D.; Etcheberry, A.; Busardo, D.; Rousseau, S.; Blanchard, G.; Moral, N.; Bruma, A.; et al. Surface Modification of Nanocatalysts via Ion Beam Techniques for Enhanced Activity. *Appl. Catal. A Gen.* **2025**, *707*, 120536. [CrossRef]
17. Magudapathy, P.; Srivastava, S.K.; Gangopadhyay, P.; Amirthapandian, S.; Saravanan, K.; Das, A.; Panigrahi, B.K. Alloying of Metal Nanoparticles by Ion-Beam Induced Sputtering. *Chem. Phys. Lett.* **2017**, *667*, 38–44. [CrossRef]
18. Fu, K.; Zeng, L.; Liu, J.; Liu, M.; Li, S.; Guo, W.; Gao, Y.; Pan, M. Magnetron Sputtering a High-Performance Catalyst for Ultra-Low-Pt Loading PEMFCs. *J. Alloys Compd.* **2020**, *815*, 152374. [CrossRef]
19. Wang, G.D.; Kong, D.D.; Pan, Y.H.; Pan, H.B.; Zhu, J.F. Low Energy Ar-Ion Bombardment Effects on the CeO_2 Surface. *Appl. Surf. Sci.* **2012**, *258*, 2057–2061. [CrossRef]
20. Liu, Y.; Li, F.; Tian, H.; Wang, G.; Wang, X. Influence of Ion Beam Surface Treatment on the Emission Performance of Photocathodes. *Nanoscale Adv.* **2022**, *4*, 3517–3523. [CrossRef]
21. Clark, A.H.; Marchbank, H.R.; Thompsett, D.; Fisher, J.M.; Longo, A.; Beyer, K.A.; Hyde, T.I.; Sankar, G. On the Effect of Metal Loading on the Reducibility and Redox Chemistry of Ceria Supported Pd Catalysts. *Phys. Chem. Chem. Phys.* **2022**, *24*, 2387–2395. [CrossRef]
22. Kimata, T.; Kakitani, K.; Yamamoto, S.; Shimoyama, I.; Matsumura, D.; Iwase, A.; Mao, W.; Kobayashi, T.; Yamaki, T.; Terai, T. Activity Enhancement of Platinum Oxygen-Reduction Electrocatalysts Using Ion-Beam Induced Defects. *Phys. Rev. Mater.* **2022**, *6*, 035801. [CrossRef]
23. Wan, W.; Geiger, J.; Berdunov, N.; Lopez Luna, M.; Chee, S.W.; Daelman, N.; López, N.; Shaikhutdinov, S.; Roldan Cuenya, B. Highly Stable and Reactive Platinum Single Atoms on Oxygen Plasma-Functionalized CeO2 Surfaces: Nanostructuring and Peroxo Effects. *Angew. Chem. Int. Ed.* **2022**, *61*, e202112640. [CrossRef]
24. Zlobin, V.N.; Bannikov, M.G.; Vasilev, I.P.; Cherkasov, J.A.; Gawrilenko, P.N. Potential of Use of Ion Implantation as a Means of Catalyst Manufacturing. *Proc. Inst. Mech. Eng. Part D J. Automob. Eng.* **2002**, *216*, 385–390. [CrossRef]
25. Qu, J.; Liu, W.; Liu, R.; He, J.; Liu, D.; Feng, Z.; Feng, Z.; Li, R.; Li, C. Evolution of Oxygen Vacancies in Cerium Dioxide at Atomic Scale under CO2 Reduction. *Chem. Catal.* **2023**, *3*, 100759. [CrossRef]
26. Wolf, G.K. Chemical and Catalytic Effects of Ion Implantation. *Radiat. Eff.* **2006**, *65*, 107–116. [CrossRef]
27. Machida, M.; Taniguchi, H.; Kijimaa, T.; Nakatanib, J. Methane Combustion Activity of Alumina Supported Pt, Pd, and Rh Modified by High-Energy Ion Beam Irradiation. *J. Mater. Chem.* **1998**, *8*, 781–785. [CrossRef]
28. Shah, P.M.; Burnett, J.W.H.; Morgan, D.J.; Davies, T.E.; Taylor, S.H. Ceria–Zirconia Mixed Metal Oxides Prepared via Mechanochemical Grinding of Carbonates for the Total Oxidation of Propane and Naphthalene. *Catalysts* **2019**, *9*, 475. [CrossRef]
29. Parthasarathi, B.; Priolkar, R.K.; Gayen, A.; Sarode, P.R.; Hegde, M.S.; Emura, S.; Kumashiro, R.; Jayaram, V.; Subbanna, G.N. Ionic Dispersion of Pt over CeO_2 by the Combustion Method Structural Investigation by XRD, TEM, XPS, and EXAFS. *Chem. Mater.* **2003**, *15*, 2049–2060. [CrossRef]

30. Liotta, L.F.; Longo, A.; Macaluso, A.; Martorana, A.; Pantaleo, G.; Venezia, A.M.; Deganello, G. Influence of the SMSI Effect on the Catalytic Activity of a Pt(1%)/$Ce_{0.6}Zr_{0.4}O_2$ Catalyst: SAXS, XRD, XPS and TPR Investigations. *Appl. Catal. B* **2004**, *48*, 133–149. [CrossRef]
31. Ji, Y.; Xu, D.; Bai, S.; Graham, U.; Crocker, M.; Chen, B.; Shi, C.; Harris, D.; Scapens, D.; Darab, J. Pt- and Pd-Promoted CeO_2-ZrO_2 for Passive NO_x Adsorber Applications. *Ind. Eng. Chem. Res.* **2017**, *56*, 111–125. [CrossRef]
32. Romeo, M.; Bak, K.; El Fallah, J.; Le Normand, F.; Hilaire, L. XPS Study of the Reduction of Cerium Dioxide. *Surf. Interface Anal.* **1993**, *20*, 508–512. [CrossRef]
33. Osazuwa, O.U.; Ng, K.H. The Roles of Oxygen Mobility and Oxygen Vacancy in Metallic Catalysts-Prompted Dry Reforming of Methane: A Review. *Renew. Energy* **2026**, *256*, 124074. [CrossRef]
34. Wisniewska, J.; Ziolek, M.; Artioli, N.; Daturi, M. The Effect of Niobium and Tantalum on Physicochemical and Catalytic Properties of Silver and Platinum Catalysts Based on MCF Mesoporous Cellular Foams. *J. Catal.* **2016**, *336*, 58–74. [CrossRef]
35. Kalia, S.; Salim, A.; Bala, R.; Singh, R.K.; Singhal, R.; Dhiman, R. Low Energy Ag Ion Irradiation-Induced Surface Modification Studies of Au-Graphene Oxide Nanocomposite Thin Films. *Thin Solid Films* **2023**, *772*, 139802. [CrossRef]
36. Colo, G.; Pijolat, M.; Valdivieso, F.; Vidal, H.; Kas-Par, J.; Finocchio, E.; Daturi, M.; Binet, C.; Lavalley, J.C.; Bakerd, R.T.; et al. Surface and Structural Characterization of Ce x $Zr_{1-x}O_2$ CEZIRENCAT Mixed Oxides as Potential Three-Way Catalyst Promoters. *J. Chem. Soc. Faraday Trans.* **1998**, *94*, 3717–3726. [CrossRef]